OPEN ACCESS

REPORT

Orbital torque switching of perpendicular magnetization in Ti/ferrimagnet bilayers

Teng Xu,[1,*] Aihua Tang,[1] Kang Wang,[1] Wensen Wei,[1] Yizhou Liu,[1,2] and Haifeng Du[1,2,*]

*Correspondence: txu@hmfl.ac.cn (T.X.); duhf@hmfl.ac.cn (H.D.)

Received: June 6, 2025; Accepted: August 18, 2025; Published Online: August 22, 2025; https://doi.org/10.59717/j.xinn-mater.2025.100158

GRAPHICAL ABSTRACT

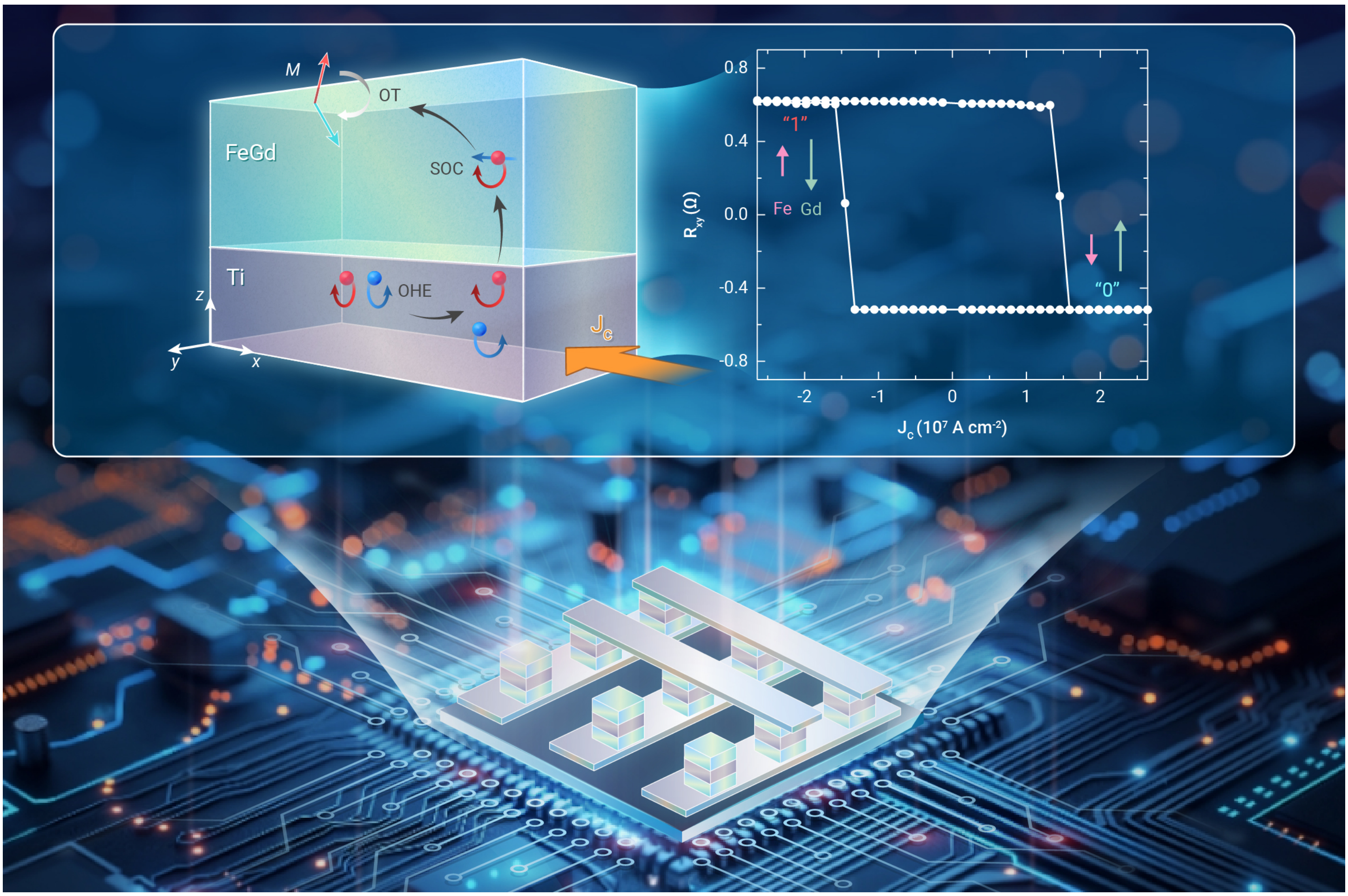

PUBLIC SUMMARY

- The orbital torque switching of perpendicular magnetization is achieved in Ti/ferrimagnet bilayer.
- The current-induced orbital torque originates from the bulk orbital Hall effect in the light metal Ti.
- The torque efficiency increases four-fold by enhancing the spin-orbit coupling in $Fe_{1-x}Gd_x$ ferrimagnets.

REPORT

OPEN ACCESS

Orbital torque switching of perpendicular magnetization in Ti/ferrimagnet bilayers

Teng Xu,[1,*] Aihua Tang,[1] Kang Wang,[1] Wensen Wei,[1] Yizhou Liu,[1,2] and Haifeng Du[1,2,*]

[1]Anhui Province Key Laboratory of Low-Energy Quantum Materials and Devices, High Magnetic Field Laboratory, HFIPS, Chinese Academy of Sciences, Hefei 230031, China

[2]Science Island Branch of Graduate School, University of Science and Technology of China, Hefei 230026, China

*Correspondence: txu@hmfl.ac.cn (T.X.); duhf@hmfl.ac.cn (H.D.)

Received: June 6, 2025; Accepted: August 18, 2025; Published Online: August 22, 2025; https://doi.org/10.59717/j.xinn-mater.2025.100158

Citation: Xu T., Tang A., Wang K., et al. (2025). Orbital torque switching of perpendicular magnetization in Ti/ferrimagnet bilayers. *The Innovation Materials* **3**:100158.

Orbital torque, associated with orbital current, enables light metals to efficiently manipulate magnetization with rich tunability. A clear demonstration of perpendicular magnetization switching using light metals alone is essential for understanding orbital physics and developing high-density orbitronic devices. Here, we report orbital torque switching of perpendicular magnetization of ferrimagnet ($Fe_{1-x}Gd_x$) using Ti 3d light metal alone. The torque efficiency increases four-fold by enhancing the spin-orbit coupling in $Fe_{1-x}Gd_x$ through modulating Gd composition, which is a characteristic feature of orbital torque. Our findings demonstrate that light metals in combination with rare earth-transition metal ferrimagnets can be employed for efficient orbitronic devices and serve as a model system for studying orbitronics.

INTRODUCTION

Achieving effective control of magnetization through electrical means is central to modern information technology.[1-3] Methods harnessing the electron's spin angular momentum, such as the spin-orbit torque (SOT), have already facilitated vast device applications.[4-7] Recently, the electron's orbital degree of freedom has sparked attention as an emergent way to manipulate magnetization, known as orbital torque (OT).[8-10] OT is associated with orbital current generated by either interfacial or bulk effect, e.g., the orbital Hall effect (OHE). In the case of OHE, an external electric field induces a transverse orbital current, which can then be converted into spin angular momentum and exert an OT on the magnetization.[11-24] The generation of orbital current does not require spin-orbit coupling (SOC), so even 3d light metal (LMs), such as Ti, can be utilized as sources of OT.[25,26]

As depicted in Figure 1A, OT typically comprises three main processes: charge-to-orbital conversion, orbital-to-spin conversion, and spin-to-magnetization transfer. The OHE serves as a method for generating orbital current via charge current. The polarization direction of the orbital current is determined by the sign of the intrinsic orbital Hall angle (θ_{OH}) of LMs. Subsequently, the orbital current is injected into the adjacent magnets, where orbital-to-spin conversion occurs due to the SOC of the magnetic material. Finally, the resultant spin current interacts with local magnetizations via exchange coupling, thereby generating torque. OT has already been characterized in various LM-magnetic bilayers/multilayers.[20,21,23,27-30] It has been shown that the torque efficiency of LMs is comparable or even greater than that of traditional heavy metals (HMs, such as Ta, Pt, and Ir) usually employed for SOT.[11,12,15,31] The correlation between OT and the adjacent magnetic layer's SOC also provides a new avenue for enhancing the torque efficiency.[17,18] Therefore, LMs can control magnetization with the advantages of being environmentally friendly and low-cost due to the diverse material choices.

To realize high-density orbitronic applications with OT and further unlock its technological potential, it is crucial to demonstrate the switching of perpendicular magnetization with 3d LMs alone.[9,10] Previous efforts have employed LM/HM/ferromagnet multilayers and 4d Zr-magnetic bilayers/multilayers (such as Cr/Pt/CoFeB, Zr/[Co/Pt]$_3$ and Zr/CoFeB/Gd/CoFeB), where large torque efficiency and magnetization switching has been identified.[21,22,32-35] However, the sign changes of the measured torques and the use of HMs or 4d LMs make it difficult to distinguish the contributions of OT and SOT as well as the other contributions, such as self-torques and the Oersted field. Recently, the OHE and orbital pumping effect have been discovered in the typical 3d LM Ti.[25,36] However, a clear demonstration of an OT switching of perpendicular magnetization via 3d LMs alone remains elusive. More importantly, the strong SOC correlation, which is a key feature of OT, and tunability of OT efficiency from the magnet side have also not been well explored in the magnetization switching.

Here, we report on OT in 3d light metal/ferrimagnet (Ti/$Fe_{1-x}Gd_x$) bilayers that are large enough to induce full switching of the perpendicular magnetization in the absence of traditional HMs. The OT efficiency, extracted via harmonic voltage measurement, shows that it is dominated by the bulk orbital Hall effect (OHE). Furthermore, the rare earth-transition metal (RE-TM) ferrimagnet (FIM) employed here enables additional control of its SOC while maintaining almost identical magnetic parameters. Taking advantage of this feature, we found that the OT efficiency in Ti/$Fe_{1-x}Gd_x$ shows a four-fold increase when the ferrimagnetic layer's SOC is enhanced, which is a key characteristic of OT. Our results show that LMs alone can switch perpendicular magnetization with great tunability from the magnet side.

MATERIALS AND METHODS

Magnetic multilayers of stacking order Ti(t_{Ti})/$Fe_{0.70}Gd_{0.30}$(10)/Si_3N_4(5), Si_3N_4(5)/$Fe_{0.70}Gd_{0.30}$(10)/Ti(10), Ti(10)/$Fe_{0.80}Gd_{0.20}$(10)/Si_3N_4/(5), Si_3N_4(5)/$Fe_{0.70}Gd_{0.30}$(10)/Si_3N_4(5) (number denotes the thickness in nanometer) are fabricated on thermally oxidized silicon substrates by using ultrahigh vacuum magnetron sputtering system (AJA Orion 8). The base pressure of the main chamber is better than 1×10^{-8} Torr and the Ar pressure is at 3 mTorr. A 1 nm Ta layer is used as an adhesive layer and an upper insulating Si_3N_4 (5 nm) layer is used for preventing oxidization, respectively. Notably, compared to 1 nm-thick Ta adhesive layers, the much thicker Ti and FeGd layers are more electrically conductive, allowing most of the charge current to flow through them. The $Fe_{1-x}Gd_x$ FIM layers are synthesized by co-sputtering the Fe and Gd targets, in which the atomic ratio (x) can be adjusted by fixing the growth power of the Fe target while changing the growth power of the Gd target. The chemical composition of the deposited $Fe_{0.70}Gd_{0.30}$ FIM layers can be determined by the deposition rates of the Fe and Gd targets, which can measured using the in-situ thickness monitor in the magnetic sputtering chamber. Notably the deposition condition of $Fe_{1-x}Gd_x$ FIM layers are maintained the same for the Ti(t_{Ti})/$Fe_{0.70}Gd_{0.30}$(10)/Si_3N_4(5) multilayers with various Ti thickness. Magnetic multilayers were patterned into Hall bar devices with a channel width of 20 μm by utilizing standard photolithography and Ar ion milling. The contact electrodes are made of Ta/Pt (20 nm/50 nm). The interface and crystalline structure of the multilayers were examined using cross-sectional scanning transmission electron microscopy (STEM, Thermo Fischer Scientific Themis Z) operated at 300 kV. Thin section of the grown film are prepared using a focused ion beam (FIB) system. Energy dispersive X-ray spectroscopy (EDS) measurements are conducted to further confirm the chemical composition of the FeGd ferrimagnetic alloy (Figure S1). The magnetic hysteresis loops were measured by using a magnetic property measurement system (MPMS, Quantum Design) with a maximum magnetic field of 7T. The magnetic fields were applied along the in-plane and out-of-plane direction at room temperature. The anomalous and planar Hall effect (AHE) measurements were performed by using a home-built electrical transport measurement system, in which the maximum magnetic field is 2T. For all electrical transport measurements, standard Hall bar configuration was adopted and the electric current was set along the x axis. The current-induced magnetization switching is performed by injecting current pulses of duration 1 ms into the Hall bar devices and the corresponding AHE resistances were detected using a lock-in amplifier (SR830). A low alternating-current (ac) harmonic measurement using the lock-in technique is employed

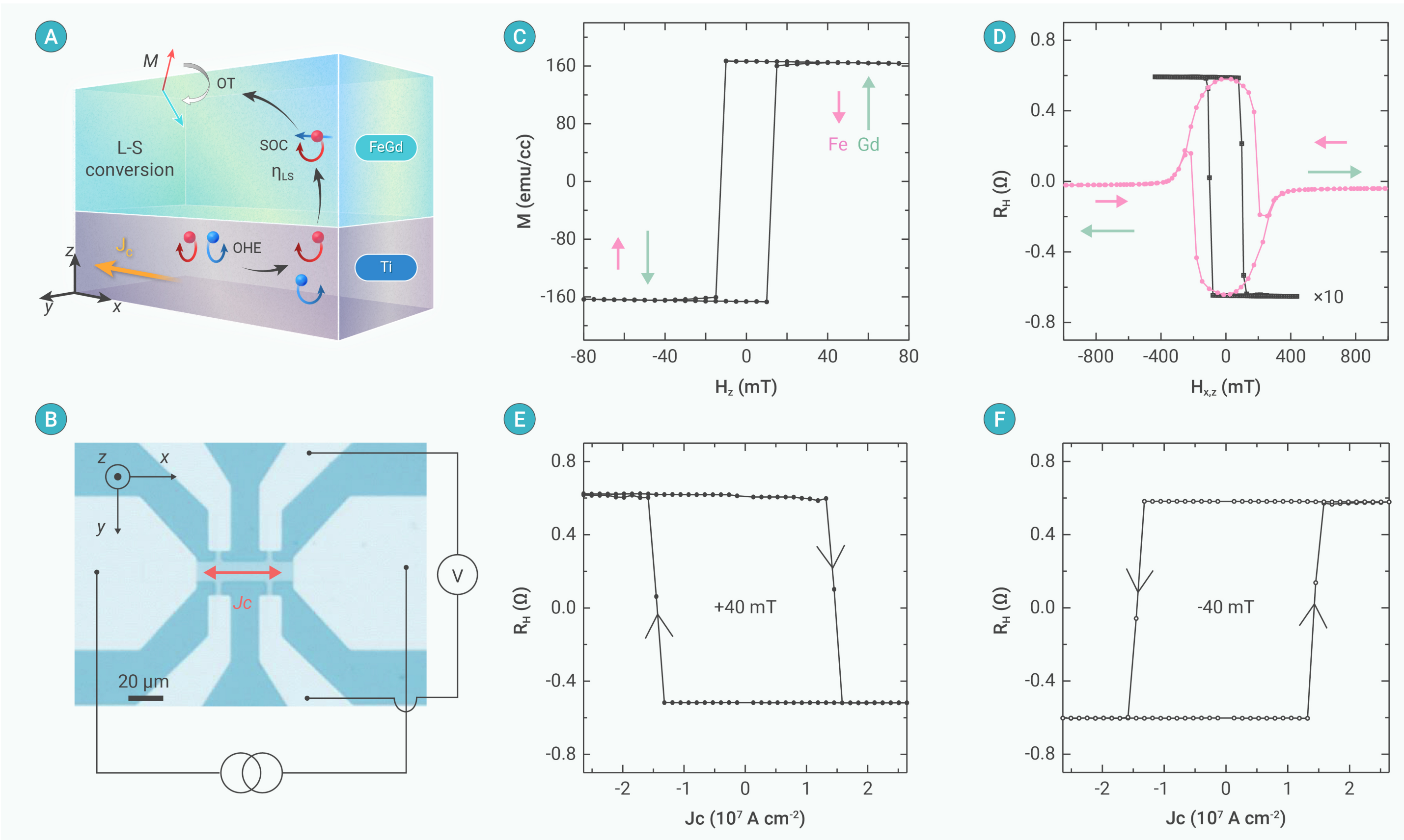

Figure 1. Perpendicular magnetization switching with Ti (A) Schematic of the OT switching of perpendicular magnetization in Ti/ferrimagnet bilayer. The orbital current is generated through the OHE in Ti, which is then injected into the adjacent ferrimagnet. The orbital-to-spin current conversion is directly achieved due to the moderate SOC of Gd. Lastly, the converted spin current interacts with the local magnetization through the exchange coupling and gives rise to the OT. η_{LS} denotes the orbital-to-spin current conversion efficiency related to SOC of ferrimagnet. (B) Optical image of the Hall bar device and the corresponding measurement configuration. (C) The OOP magnetic hysteresis loop for the Ti(10)/$Fe_{0.70}Gd_{0.30}$(10) sample. (D) The corresponding anomalous Hall loops measured with OOP (black) and IP (red) field sweeping. The pink (green) arrow denotes the spin orientation of Fe (Gd) magnetic sublattice. (E-F) The current-induced magnetization switching curves under an in-plane field $H_x = +40mT$ and $H_x = -40mT$. The arrows denote the switching polarities.

and two lock-in amplifiers are used to simultaneously record the first and second harmonic signals. The frequency of the ac current is 233 Hz. The applied low ac current can effectively avoid the thermoelectric contribution in the harmonic signals.

RESULTS AND DISCUSSION

Perpendicular magnetization switching with Ti

To demonstrate the OT-induced perpendicular magnetization switching, a typical 3d LM Ti is employed. Ti exhibits negligible spin Hall conductivity due to its negligible SOC, yet it has a large orbital Hall conductivity.[11,12,15,23-25] Ti/ferrimagnet bilayers with stacking order Ti(10)/$Fe_{0.70}Gd_{0.30}$(10)/Si_3N_4(5) were first fabricated on thermally oxidized silicon substrates. The $Fe_{1-x}Gd_x$ alloy is a typical RE-TM ferrimagnet with two inequivalent and antiparallel magnetic sublattices. A finite net magnetization remains because of the uncompensated magnetic moments from the oppositely aligned sublattices.[37-39] The magnetic properties of $Fe_{1-x}Gd_x$ ferrimagnets are highly tunable through the chemical compositions. The $Fe_{0.70}Gd_{0.30}$ composition is magnetically Gd-dominant in which the Gd sublattice is parallel with the net magnetization. The samples were patterned into Hall bar devices as shown in Figure 1B, which also illustrates the measurement configuration. The out-of-plane magnetic hysteresis loop M−H (Figures 1C & S2-S3) and the anomalous Hall effect (AHE) loop $R_H - H$ (Figure 1D) indicate that the ferrimagnet possesses strong perpendicular magnetic anisotropy (PMA). The Hall resistance (R_H) is predominantly attributed to the anomalous Hall effect, as determined by the measured transverse voltage in Hall bar devices. The values of the anomalous Hall resistance R_H remain nearly constant at zero field in both out-of-plane (OOP) and in-plane (IP) measurement configurations. This is attributed to the strong perpendicular magnetic anisotropy (PMA) of the $Fe_{0.70}Gd_{0.30}$ ferrimagnetic layers. The jump in the $R_H - H_x$ loop arises from the abrupt magnetization switching during continuous sweeping of the in-plane field H_x, a phenomenon caused by the slight misalignment of H_x within the film plane.

Next, we examine the OT-induced magnetization switching in Ti(10)/$Fe_{0.70}Gd_{0.30}$ device. Due to the strong SOC of Gd, the orbital current injected from the Ti layer can be converted into spin current, which further applies a torque on the local (net) magnetic moments of the ferrimagnet. During the current-induced OT switching measurements, a series of current pulses with varied amplitude and fixed duration were applied along longitudinal direction (x axis) of Hall bar devices. The current pulses have a maximum amplitude of 80 mA and a duration of 1 ms. In between two adjacent current pulses, the magnetization states of the $Fe_{0.70}Gd_{0.30}$ can be inferred from the R_H. The interval between successive current pulses is set to be 4 s, which is significantly longer than the pulse duration. This combination of short pulse duration and extended interval helps to reduce current-induced Joule heating. A longitudinal in-plane magnetic field (H_x) was simultaneously applied along the current pulse direction, which is required for realizing a deterministic switching. When J_c flows in the x-direction, the system's symmetry with respect to the x-z plane is preserved in the absence of H_x, which does not allow deterministic switching. In contrast, applying H_x breaks the inversion symmetry, enabling deterministic switching of perpendicular magnetization.[40,41] Note that the current density in Ti layers (J_c) can be estimated through the parallel resistor model (Figure S4).

Figures 1E-F show the Hall resistance as a function of the current pulse with varying amplitudes under a fixed $H_x = +40mT$ and $-40mT$, respectively. Compared with field-driven R_H change, nearly complete current-induced switching is realized just by injecting a series of current pulses. H_x is much smaller than the magnetic anisotropy field (H_k), and the slight misalignment of H_x is insufficient to induce abrupt magnetization switching.

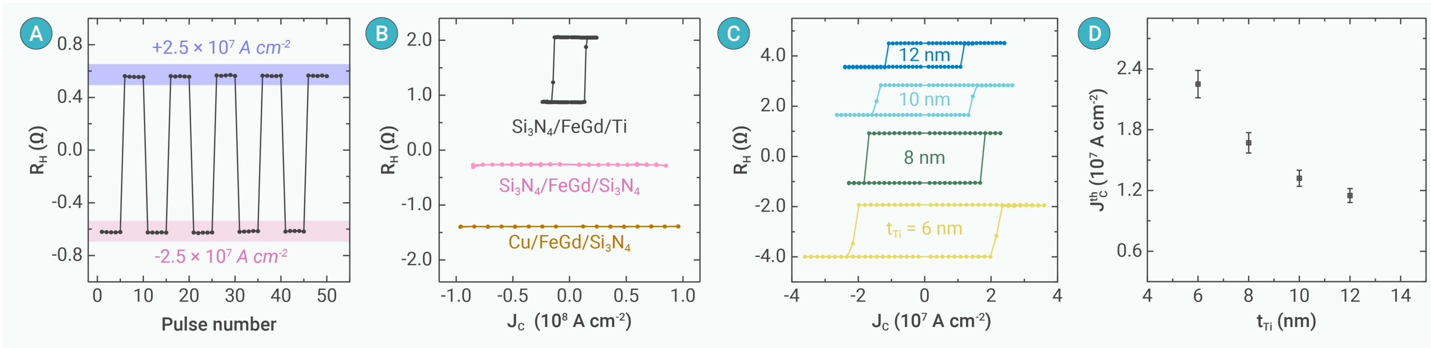

Figure 2. Thickness dependence of the orbital torque switching (A) Repeatable magnetization switching by a series of current pulses of $\pm 2.5\times10^{7}Acm^{-2}$ at $H_x=-40mT$. (B) The current-induced magnetization switching curves for the inverted $Si_3N_4/Fe_{0.70}Gd_{0.30}/Ti$, $Si_3N_4/Fe_{0.70}Gd_{0.30}/Si_3N_4$, and $Cu/Fe_{0.70}Gd_{0.30}/Si_3N_4$ stacking at $H_x=+40mT$. (C) Current-induced magnetization switching curves for $Ti(t_{Ti})/Fe_{0.70}Gd_{0.30}/Si_3N_4$ multilayers with varying Ti thickness at $H_x=-40mT$. (D) The evolution of the critical switching current density J_C^{th} as a function of Ti thickness.

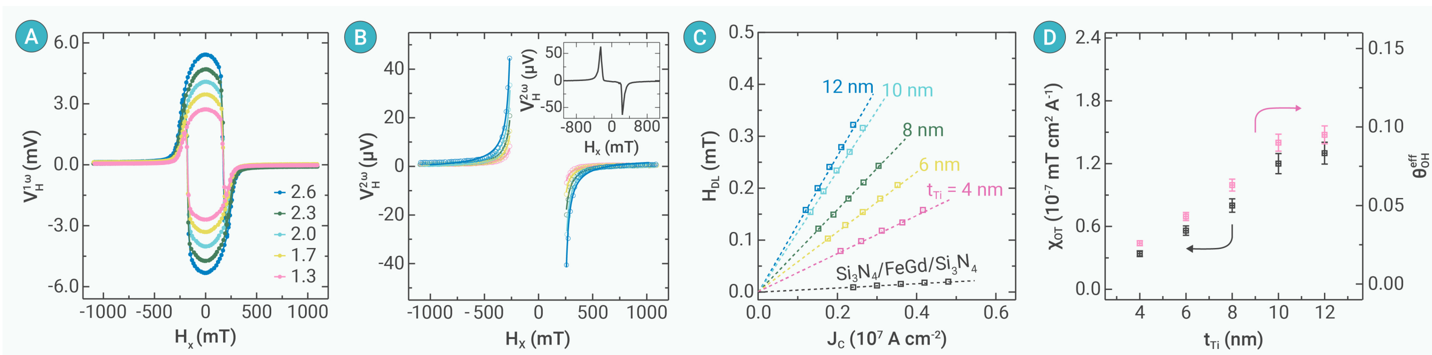

Figure 3. Determination of orbital torque efficiency (A) First harmonic Hall voltage $V_H^{1\omega}$ as a function of the longitudinal magnetic field H_x for $Ti(10)/Fe_{0.70}Gd_{0.30}(10)$ at different current densities. The unit of the current density is 10^6 A·cm^{-2}. (B) The corresponding second harmonic Hall voltage $V_H^{2\omega}$ as a function of the longitudinal magnetic field H_x at different current densities. The inset displays the harmonic signal across the entire filed range. (C) The current density J_C dependence of the damping-like effective field H_{DL} for $Ti(t_{Ti})/Fe_{0.70}Gd_{0.30}(10)/Si_3N_4$ samples with varying Ti thickness and $Si_3N_4/Fe_{0.70}Gd_{0.30}(10)/Si_3N_4$ sample. (D) The orbital torque efficiency χ_{OT} and the effective orbital Hall angle θ_{OH}^{eff} as a function of Ti thickness t_{Ti}.

Notably, if the slight misalignment of the fixed H_x is critical, deterministic switching cannot be achieved just by injecting a series of current pulses. The critical switching current density J_C^{th} is $1.5\times10^{7}Acm^{-2}$. The value is comparable to those originally reported for the SOT-driven switching in HM/ferromagnet devices.[42-44] Figure 2A further illustrates the current-induced magnetization switching cycles in the $Ti(10)/Fe_{0.70}Gd_{0.30}$ device, indicating the high repeatability and stability of the OT switching. The current-induced switching reverses its polarity after applying opposite in-plane field, which is consistent with the symmetry of OT. Additionally, the critical switching current density reduces with increased H_x (Figures S5-S7), which occurs because of the reduced energy barrier between up and down magnetization states.

To verify the crucial role of Ti, control film stack of $Si_3N_4/Fe_{0.70}Gd_{0.30}(10)/Ti(10)$ and the corresponding devices were fabricated and examined. Similar to the spin Hall effect, the orbital Hall effect generates a purely z-axis-flowing orbital current when a charge current is injected along the x-axis. Notably, orbital currents with opposite polarizations (+y and -y) accumulate at the top and bottom interfaces of the Ti layer, respectively. For the inverted film stack, the OT should reverse its sign due to the opposite polarization of orbital current generated in Ti layer and so does the switching polarity. As shown in Figure 2B, the experimental switching polarity reverses the sign compared with the original film stack as expected.

To further rule out other possible effects, such as self-torques and the Oersted field, we fabricated and examined $Si_3N_4/Fe_{0.70}Gd_{0.30}(10)/Si_3N_4$ and $Cu/Fe_{0.70}Gd_{0.30}(10)/Si_3N_4$ samples and devices. As shown in Figure 2B, no magnetization switching was observed in either sample. Furthermore, the energy dispersive spectroscopy (EDS) element mapping demonstrates that there is no obvious variation in the chemical composition along the thickness direction of $Fe_{0.70}Gd_{0.30}$ layer (Figure S8). Hence, the recently discovered self-torque in RE-TM ferrimagnets can be excluded.[45-48] Notably, the Cu material possess negligible SHE and OHE.[31] This not only excludes the dominated role of the self-torque but also signifies the critical role of the orbital Hall material Ti. Additionally, the Cu material is more electrically conductive and the Oersted field effect can be enhanced in the measured OT device. However, the perpendicular magnetization of FeGd ferrimagnet cannot be switched by the enhanced Oersted field, which directly excludes the role of the Oersted field.

In order to compare OT with SOT, we deposited and patterned a $Pt/Fe_{0.70}Gd_{0.30}/Si_3N_4$ multilayer into a standard Hall bar device. Pt, a typical spin source material, generates spin current via the SHE.[43,49,50] Under the same measurement configuration, current-induced SOT switching was observed. Compared to the field-driven AHE resistance change (ΔR_H), nearly full current-induced switching can also be achieved by conventional SOT (Figure S9). The critical switching current density J_C^{th} is approximately $1.3\times10^{7}Acm^{-2}$, comparable to values for OT-driven switching in $Ti/Fe_{0.70}Gd_{0.30}$ devices. The spin Hall angle (θ_{sh}) of the Pt spin source material has been reported to be about ~0.1, which is similar to the measured effective orbital Hall angle discussed in the following section.[49,50] Additionally, the critical switching current density in $Ti/Fe_{0.70}Gd_{0.30}$ samples is also comparable to that in Pt/FeTb sample.[51] This demonstrates that Ti, a 3d LM, can serve as an efficient orbital Hall material, rivaling typical 5d heavy metals. To confirm the universal OT in LM/FeGd bilayer, we have further performed OT switching in $V/Fe_{0.80}Gd_{0.30}$ and $Cr/Fe_{0.80}Gd_{0.30}$ samples. OT-induced deterministic full switching can also be achieved (Figure S10).

Thickness dependence of the orbit torque switching

To further characterize the OT, current-induced switching measurements were performed in other $Ti(t_{Ti})/Fe_{0.70}Gd_{0.30}$ devices with varying the Ti thickness. The varying thickness of the Ti layer has a negligible effect on the PMA of the $Fe_{0.70}Gd_{0.30}$ ferrimagnetic films, as confirmed by magnetometry and anomalous Hall measurements (Figure S1). As shown in Figure 2C, deterministic OT switching can be achieved in all $Ti(t_{Ti})/Fe_{0.70}Gd_{0.30}$ devices under an in-plane external field $H_x=-40mT$. Their corresponding switching curves with

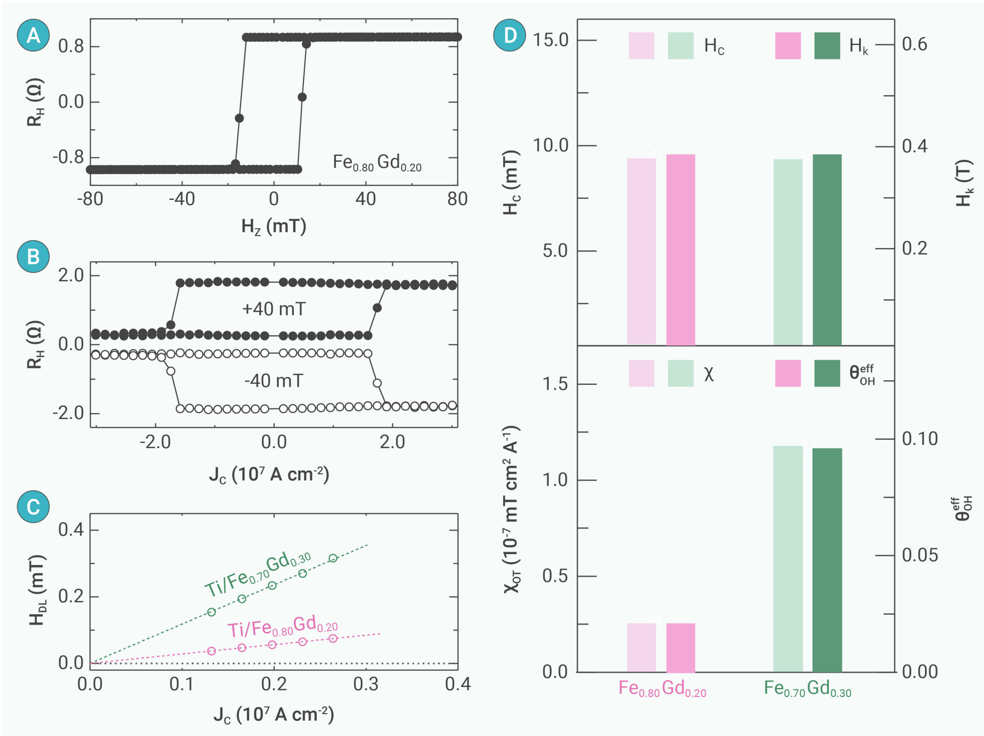

Figure 4. Correlation between orbital torque and spin-orbit coupling (A) The anomalous Hall loops for Ti(10)/$Fe_{0.80}Gd_{0.20}$(10) sample. (B) The corresponding current-induced magnetization switching curves under $H_x = \pm 40mT$. (C) The current density J_C dependence of the damping-like effective field H_{DL} for Ti(10)/$Fe_{0.70}Gd_{0.30}$(10) and Ti(10)/$Fe_{0.80}Gd_{0.20}$(10) samples. (D) The coercive field H_C and magnetic anisotropy field H_k for both samples in top panel and the corresponding orbital torque efficiency χ_{OT} and effective orbital Hall angle θ_{OH}^{eff} in bottom panel.

sign reversal at $H_x = +40mT$ can be found in Figure S7. A deterministic switching cannot be achieved in in Ti(4 nm)/$Fe_{0.70}Gd_{0.30}$/Si_3N_4 sample due to its low OT efficiency, which is further confirmed in the following part. The critical switching current density (J_C^{th}) reduces to $1.0 \times 10^7 Acm^{-2}$ with the Ti thickness up to 12 nm, as illustrated in Figure 2D. Compared to the low J_C^{th} observed in the Zr/CoFeB/Gd/CoFeB sample, the higher critical switching current density in the present Ti/$Fe_{0.70}Gd_{0.30}$ sample may stem from lower orbital torque efficiency.[35] This could be attributed to the relatively low SOC in the $Fe_{0.70}Gd_{0.30}$. Additionally, recent reports indicate that interface transparency to orbital currents significantly impacts OT.[52] Since interface transparency can vary across different material systems, this variation could also contribute to the difference in critical switching current density. Furthermore, the $Fe_{0.70}Gd_{0.30}$ ferrimagnetic layer switched by OT in our study is approximately 10 nm thick, which is considerably thicker than the CoFeB/Gd/CoFeB layer (~3 nm). This increased thickness may further contribute to the higher switching current density observed in the Ti/$Fe_{0.70}Gd_{0.30}$ devices.

The harmonic Hall voltage measurements were performed to quantify the OT efficiency by using a low-current excitation lock-in technique. We applied a low-frequency ac current to the Hall bar and simultaneously measure the first harmonic ($V_H^{1\omega}$) and second harmonic ($V_H^{2\omega}$) Hall voltage with two lock-in amplifiers by sweeping H_x. When a sinusoidal current is applied, the current-induced effective field oscillates in sync with the applied current. Based on the macrospin model, the oscillating effective fields induce small oscillation of the magnetization about its equilibrium direction, generating a second harmonic contribution to the Hall voltage.[53-56] The first harmonic Hall term ($V_H^{1\omega}$) relates to the equilibrium direction of the magnetization and is independent of the effective fields. The second harmonic term ($V_H^{2\omega}$) measures the susceptibility of the magnetization to the current-induced effective fields. In general, the effective filed can be decomposed into the damping-like field H_{DL} and field-like field H_{FL}. When H_x is larger than the anisotropy field H_k, the magnetization is nearly aligned along the external field and the secondary harmonic Hall voltage signals can be written as

$$V_H^{2\omega} = \frac{V_{AHE}}{2}\frac{H_{DL}}{|H_x - H_k|} + V_{PHE}\frac{H_{FL}}{|H_x|} + V_{thermal}\frac{H_x}{|H_x|} \quad (1)$$

where the V_{AHE} and V_{PHE} are the anomalous Hall and planar Hall voltage and $V_{thermal}$ is the thermal contribution from the anomalous Nernst and spin Seebeck effects.[57-60] Note that the thermal contributions can be measured and separated by studying the field dependence of $V_H^{2\omega}$ in the high field limit (Figure S11). In addition, since the V_{PHE} is much smaller than V_{AHE} for the perpendicular FeGd ferrimagnets, the second term can be neglected. Thus, the effective damping-like field H_{DL} is mostly relevant to the current-induced magnetization switching.

Figures 3A-B show the first and second harmonic Hall voltage ($V_H^{1\omega}$ and $V_H^{2\omega}$) of Ti(10)/$Fe_{0.70}Gd_{0.30}$(10)/Si_3N_4 sample as a function of H_x at different current densities, respectively. As shown in Figure 3A, the net magnetization is aligned along the in-plane direction when H_x is larger than H_k. Through fitting the $V_H^{2\omega} - H_x$ curves with the equation (1), the effective damping-like field (H_{DL}) can be acquired. The first and second harmonic Hall signals for other samples of various Ti thickness can be found in Figures S12-S15. The variations of the H_{DL} as a function of the current density in all samples are summarized in Figure 3C. By a linear fitting, the OT efficiency ($\chi_{OT} = H_{DL}/J_c$) can be determined. Figure 3D shows the evolution of OT efficiency with the Ti thickness. As Ti thickness increases, the orbital torque efficiency first increases and then saturates at $t_{Ti} \approx 10$nm. The increase of χ_{OT} with increasing the Ti thickness suggests that the OT is dominated by the bulk effect rather than the interfacial effect such as the orbital Rashba-Edelstein effect.[61-64] When the Ti thickness is 12 nm, the OT efficiency reaches $1.3 \times 10^{-7} mTcm^2A^{-1}$. This increasing OT efficiency is consistent with the decreasing critical switching current density with Ti thickness shown in Figure 2D.

The effective orbital Hall angle (θ_{OH}^{eff}) can be estimated by using $\theta_{OH}^{eff} = 2e/\hbar \cdot M_s \cdot t_{FeGd} \cdot \chi_{OT}$, where e is the electron charge, $\hbar$ is the reduced Planck constant, M_s (~163 emu/cc) is the saturation magnetization and t_{FeGd} (~10 nm) is the ferrimagnetic layer thickness. As shown in Figure 3D, the θ_{OH}^{eff} have a similar trend with the orbital torque efficiency. The θ_{OH}^{eff} first increases and then saturate at a maximum value as t_{Ti} exceeds the orbital diffusion length. The orbital diffusion length (~10 nm) in Ti is much longer the spin diffusion length (~4 nm) in Pt.[49,50] The θ_{OH}^{eff} approaches 0.1 when the Ti thickness is increased to 12 nm. This value is comparable to the reported effective spin Hall angle of traditional HMs like Pt, suggesting the OT to be an efficient way to switch perpendicular magnetization.

Correlation between orbit torque and spin-orbit coupling

A key feature of the OT is its correlation with SOC of the magnetic layer, as the orbital current is converted to the spin current via the SOC. Therefore, the effective orbital Hall angle ($\theta_{OH}^{eff} = \theta_{OH} \cdot \eta_{LS}$) is not only determined by the intrinsic orbital Hall angle (θ_{OH}) of the LM, but also influenced by the orbital-to-spin conversion efficiency η_{LS}. Notably, all the examined Ti(t_{Ti})/$Fe_{1-x}Gd_x$ samples in the present work nearly possess the same interface and hence, the similar interface transparency to the orbital current. Since η_{LS} is related to the SOC of the magnetic layer, the OT can be probed and tuned through the chemical composition of the ferrimagnetic alloys in Ti/$Fe_{1-x}Gd_x$ magnetic bilayers. This is in stark contrast to the conventional SOT, where the role of the magnetic material choice is less important.

To investigate the SOC correlation of OT, the film stack of Ti(10)/$Fe_{0.80}Gd_{0.20}$(10) with less Gd content was also fabricated through the same growth condition. The $Fe_{0.80}Gd_{0.20}$ composition is magnetically Fe-dominated, which is contrast to the Gd-dominant $Fe_{0.70}Gd_{0.30}$. As shown in Figure 4A, the polarity of the AHE loop for $Fe_{0.80}Gd_{0.20}$ is opposite to that of $Fe_{0.70}Gd_{0.30}$

(Figure 1D). This is because the dominance of the spin-dependent transport property from the outer shell 3d magnetism of Fe element, as compared with the inner shell 4f magnetism of Gd element. So the anomalous Hall resistance mainly captures the magnetization direction of Fe.

As shown in the top panel of Figure 4D, by fine tuning the magnetic composition, $Fe_{0.80}Gd_{0.20}$ and $Fe_{0.70}Gd_{0.30}$ possess nearly the same coercive field H_c, magnetic anisotropy field H_k, and saturation magnetization M_S (Figures S2-S3). In such a case, for OT switching, the main difference between these two systems is the strength of SOC due to the different Gd composition. In contrast, similar SOT efficiency is expected with these two different compositions, which has been observed in previous works.[51,65,66]

The current-induced switching and harmonic Hall measurements were then performed in the Ti(10)/$Fe_{0.80}Gd_{0.20}$(10) device. As shown in Figure 4B, a deterministic magnetization switching is also achieved. The current density dependence of the effective damping-like field H_{DL} for both Ti/$Fe_{0.80}Gd_{0.20}$ and Ti/$Fe_{0.70}Gd_{0.30}$ samples are plotted in Figure 4C. As shown in the bottom panel of Figure 4D, despite having nearly the same magnetic properties, the OT efficiency in Ti/$Fe_{0.70}Gd_{0.30}$ is increased by four-times comparing with that in Ti/$Fe_{0.80}Gd_{0.20}$. The critical switching current density for $Fe_{0.70}Gd_{0.30}$ is also smaller than that of $Fe_{0.80}Gd_{0.20}$ due to this larger OT efficiency. The enhancement of the OT efficiency is due to the larger orbital-to-spin conversion efficiency from the increased Gd content and the corresponding larger SOC. Therefore, more efficient OT switching can be expected through increasing the Gd concentration. Such strong correlation also confirms that the current-induced switching is dominated by the OT generated by the Ti light metal. Moreover, it also demonstrates that the OT efficiency can be systematically tuned through the chemical composition of ferrimagnet in LM/ferrimagnet bilayers. Notably, tunable orbital torques have been recently demonstrated in $Co_{100-y}Gd_y/CuO_x$ bilayers with in-plane magnetization by changing the Gd content; however, OT-induced perpendicular magnetization switching remains elusive in these systems.[29]

To further confirm the SOC correlation of the OT, we fabricated and examined perpendicularly magnetized Ti/CoFeB/MgO and Ti/$[Co/Pt]_3/Si_3N_4$ control samples and their corresponding devices. No deterministic switching can be observed in the Ti/CoFeB/MgO sample, whereas it does occur in the Ti/$[Co/Pt]_3/Si_3N_4$ sample (Figures S16-S17). Given that Ti has a negligible spin Hall effect and CoFeB has minimal SOC, the perpendicular magnetization of CoFeB cannot be switched by Ti, which is consistent with previous findings.[67] For the Ti/$[Co/Pt]_3/Si_3N_4$ sample, the large SOC of $[Co/Pt]_3$ layer allows its perpendicular magnetization to be switched via OT at a low critical current density ($6.0 \times 10^6 Acm^{-2}$). Through harmonic Hall voltage measurements (Figure S18), the OT efficiency can be quantified, and the θ_{OH}^{eff} is determined to be ~0.4, which is also larger that of Ti/$Fe_{0.70}Gd_{0.30}$ device. These results further confirm the OT mechanism and indicate that the spin torque contribution of Ti is negligible. Lastly, by comparing the switching polarities and the signs of the measured torques, we determined that the sign of the SOC in $Fe_{0.70}Gd_{0.30}$ is negative (Figures S9 & S17-S18).

CONCLUSION

We have successfully realized the orbital torque-induced switching of perpendicular ferrimagnet $Fe_{1-x}Gd_x$ by utilizing a typical 3d light metal Ti without the use of traditional heavy metals. Due to the strong SOC of rare earth element Gd, an efficient orbital-to-spin current conversion can be directly achieved in $Fe_{1-x}Gd_x$ layer. The thickness dependent torque efficiency shows that the OT is dominated by the bulk orbital Hall effect of Ti. We found that the critical switching current density and orbital torque efficiency are comparable to the traditional Pt used for SOT. Furthermore, the correlation between OT and SOC of $Fe_{1-x}Gd_x$ is confirmed, making RE-TM ferrimagnetic material a versatile platform for investigating OT-related effects. Our work establishes the possibility of OT-driven perpendicular magnetization reversal utilizing 3d light metals in combination with RE-TM ferrimagnets, which is promising for developing efficient orbitronic devices.

REFERENCES

1. Žutić I., Fabian J. and Das Sarma S. (2004). Spintronics: Fundamentals and applications. *Rev. Mod. Phys.* 76:323–410. DOI:10.1103/RevModPhys.76.323
2. Fert A. (2008). Nobel lecture: Origin, development, and future of spintronics. *Rev. Mod. Phys.* 80:1517–1530. DOI:10.1103/RevModPhys.80.1517
3. Fert A., Ramesh R., Garcia V., et al. (2024). Electrical control of magnetism by electric field and current-induced torques. *Rev. Mod. Phys.* 96:015005. DOI:10.1103/RevModPhys.96.015005
4. Manchon A., Železný J., Miron I. M., et al. (2019). Current-induced spin-orbit torques in ferromagnetic and antiferromagnetic systems. *Rev. Mod. Phys.* 91:035004. DOI:10.1103/RevModPhys.91.035004
5. Han X., Wang X., Wan C., et al. (2021). Spin-orbit torques: materials, physics, and devices. *Appl. Phys. Lett.* 118:120502. DOI:10.1063/5.0039147
6. Song C., Zhang R., Liao L., et al. (2021). Spin-orbit torques: Materials, mechanisms, performances, and potential applications. *Prog. Mater Sci.* 118:100761. DOI:10.1016/j.pmatsci.2020.100761
7. Shao Q., Li P., Liu L., et al. (2021). Roadmap of spin–orbit torques. *IEEE Trans. Magn.* 57:1–39. DOI:10.1109/TMAG.2021.3078583
8. Bernevig B. A., Hughes T. L. and Zhang S.-C. (2005). Orbitronics: The intrinsic orbital current in p-doped Silicon. *Phys. Rev. Lett.* 95:066601. DOI:10.1103/PhysRevLett.95.066601
9. Go D., Jo D., Lee H.-W., et al. (2021). Orbitronics: Orbital currents in solids. *Eur. Phys. Lett.* 135:37001. DOI:10.1209/0295-5075/ac2653
10. Jo D., Go D., Choi G.-M., et al. (2024). Spintronics meets orbitronics: Emergence of orbital angular momentum in solids. *npj Spintronics* 2:19. DOI:10.1038/s44306-024-00023-6
11. Tanaka T., Kontani H., Naito M., et al. (2008). Intrinsic spin Hall effect and orbital Hall effect in 4d and 5d transition metals. *Phys. Rev. B* 77:165117. DOI:10.1103/PhysRevB.77.165117
12. Kontani H., Tanaka T., Hirashima D. S., et al. (2009). Giant orbital Hall effect in transition metals: Origin of large spin and anomalous Hall effects. *Phys. Rev. Lett.* 102:016601. DOI:10.1103/PhysRevLett.102.016601
13. Kontani H., Tanaka T., Hirashima D. S., et al. (2008). Giant intrinsic spin and orbital Hall effects in Sr_2MO_4 (M=Ru, Rh, Mo). *Phys. Rev. Lett.* 100:096601. DOI:10.1103/PhysRevLett.100.096601
14. Go D., Jo D., Kim C., et al. (2018). Intrinsic spin and orbital Hall effects from orbital texture. *Phys. Rev. Lett.* 121:086602. DOI:10.1103/PhysRevLett.121.086602
15. Jo D., Go D. and Lee H.-W. (2018). Gigantic intrinsic orbital Hall effects in weakly spin-orbit coupled metals. *Phys. Rev. B* 98:214405. DOI:10.1103/PhysRevB.98.214405
16. Sala G. and Gambardella P. (2022). Giant orbital Hall effect and orbital-to-spin conversion in 3d, 5d, and 4f metallic heterostructures. *Physical Review Research* 4:033037. DOI:10.1103/PhysRevResearch.4.033037
17. Go D. and Lee H.-W. (2020). Orbital torque: torque generation by orbital current injection. *Phys. Rev. Res.* 2:013177. DOI:10.1103/PhysRevResearch.2.013177
18. Go D., Jo D., Kim K.-W., et al. (2023). Long-range orbital torque by momentum-space hotspots. *Phys. Rev. Lett.* 130:246701. DOI:10.1103/PhysRevLett.130.246701
19. Go D., Freimuth F., Hanke J.-P., et al. (2020). Theory of current-induced angular momentum transfer dynamics in spin-orbit coupled systems. *Phys. Rev. Res.* 2:033401. DOI:10.1103/PhysRevResearch.2.033401
20. Ding S., Ross A., Go D., et al. (2020). Harnessing orbital-to-spin conversion of interfacial orbital currents for efficient spin-orbit torques. *Phys. Rev. Lett.* 125:177201. DOI:10.1103/PhysRevLett.125.177201
21. Lee D., Go D., Park H.-J., et al. (2021). Orbital torque in magnetic bilayers. *Nat. Commun.* 12:6710. DOI:10.1038/s41467-021-26650-9
22. Li T., Liu L., Li X., et al. (2023). Giant orbital-to-spin conversion for efficient current-induced magnetization switching of ferrimagnetic insulator. *Nano Lett.* 23:7174–7179. DOI:10.1021/acs.nanolett.3c02104
23. Hayashi H., Jo D., Go D., et al. (2023). Observation of long-range orbital transport and giant orbital torque. *Commun. Phys.* 6:32. DOI:10.1038/s42005-023-01139-7
24. Hayashi H., Go D., Haku S., et al. (2024). Observation of orbital pumping. *Nat. Electron.* DOI:10.1038/s41928-024-01193-1.
25. Choi Y.-G., Jo D., Ko K.-H., et al. (2023). Observation of the orbital Hall effect in a light metal Ti. *Nature* 619:52–56. DOI:10.1038/s41586-023-06101-9
26. Lyalin I., Alikhah S., Berritta M., et al. (2023). Magneto-optical detection of the orbital Hall effect in chromium. *Phys. Rev. Lett.* 131:156702. DOI:10.1103/PhysRevLett.131.156702
27. Bose A., Kammerbauer F., Gupta R., et al. (2023). Detection of long-range orbital-Hall torques. *Phys. Rev. B* 107:134423. DOI:10.1103/PhysRevB.107.134423
28. Moriya H., Taniguchi M., Jo D., et al. (2024). Observation of long-range current-induced torque in Ni/Pt bilayers. *Nano Lett.* 24:6459–6464. DOI:10.1021/acs.nanolett.3c05102
29. Ding S., Kang M.-G., Legrand W., et al. (2024). Orbital torque in rare-earth transition-metal ferrimagnets. *Phys. Rev. Lett.* 132:236702. DOI:10.1103/PhysRevLett.132.236702
30. Wang P., Feng Z., Yang Y., et al. (2023). Inverse orbital Hall effect and orbitronic terahertz emission observed in the materials with weak spin-orbit coupling. *npj Quantum Mater.* 8:28. DOI:10.1038/s41535-023-00559-6
31. Salemi L. and Oppeneer P. M. (2022). First-principles theory of intrinsic spin and orbital Hall and Nernst effects in metallic monoatomic crystals. *Phys. Rev. Mater.* 6:095001. DOI:10.1103/PhysRevMaterials.6.095001
32. Zheng Z. C., Guo Q. X., Jo D., et al. (2020). Magnetization switching driven by current-induced torque from weakly spin-orbit coupled Zr. *Phys. Rev. Res.* 2:013127. DOI:10.

1103/PhysRevResearch.2.013127
33. Xie H., Zhang N., Ma Y., et al. (2023). Efficient noncollinear antiferromagnetic state switching induced by the orbital Hall effect in chromium. *Nano Lett.* **23**:10274–10281. DOI:10.1021/acs.nanolett.3c02797
34. Zheng Z., Zeng T., Zhao T., et al. (2024). Effective electrical manipulation of a topological antiferromagnet by orbital torques. *Nat. Commun.* **15**:745. DOI:10.1038/s41467-024-45109-1
35. Yang Y., Wang P., Chen J., et al. (2024). Orbital torque switching in perpendicularly magnetized materials. *Nat. Commun.* **15**:8645. DOI:10.1038/s41467-024-52824-2
36. Hayashi H., Go D., Haku S., et al. (2024). Observation of orbital pumping. *Nat. Electron.* **7**:646–652. DOI:10.1038/s41928-024-01193-1
37. Finley J. and Liu L. (2020). Spintronics with compensated ferrimagnets. *Appl. Phys. Lett.* **116**:110501. DOI:10.1063/1.5144076
38. Zhou H.-A., Xu T., Bai H., et al. (2021). Efficient Spintronics with fully compensated ferrimagnets. *J. Phys. Soc. Jpn.* **90**:081006. DOI:10.7566/JPSJ.90.081006
39. Kim S. K., Beach G. S. D., Lee K.-J., et al. (2022). Ferrimagnetic spintronics. *Nat. Mater.* **21**:24–34. DOI:10.1038/s41563-021-01139-4
40. Yu G., Upadhyaya P., Fan Y., et al. (2014). Switching of perpendicular magnetization by spin–orbit torques in the absence of external magnetic fields. *Nat. Nanotechnol.* **9**:548–554. DOI:10.1038/nnano.2014.94
41. Liu L., Zhao T., Lin W., et al. (2023). Symmetry breaking for current-induced magnetization switching. *Appl. Physc. Rev.* **10**:021319. DOI:10.1063/5.0149290
42. Miron I. M., Garello K., Gaudin G., et al. (2011). Perpendicular switching of a single ferromagnetic layer induced by in-plane current injection. *Nature* **476**:189–193. DOI:10.1038/nature10309
43. Liu L., Lee O. J., Gudmundsen T. J., et al. (2012). Current-induced switching of perpendicularly magnetized magnetic layers using spin torque from the spin Hall effect. *Phys. Rev. Lett.* **109**:096602. DOI:10.1103/PhysRevLett.109.096602
44. Liu L., Pai C.-F., Li Y., et al. (2012). Spin-torque switching with the giant spin Hall effect of Tantalum. *Science* **336**:555. DOI:10.1126/science.1218197
45. Lee J. W., Park J. Y., Yuk J. M., et al. (2020). Spin-orbit torque in a perpendicularly magnetized ferrimagnetic TbCo single layer. *Phys. Rev. Appl.* **13**:044030. DOI:10.1103/PhysRevApplied.13.044030
46. Zheng Z., Zhang Y., Lopez-Dominguez V., et al. (2021). Field-free spin-orbit torque-induced switching of perpendicular magnetization in a ferrimagnetic layer with a vertical composition gradient. *Nat. Commun.* **12**:4555. DOI:10.1038/s41467-021-24854-7
47. Liu Q., Zhu L., Zhang X. S., et al. (2022). Giant bulk spin–orbit torque and efficient electrical switching in single ferrimagnetic FeTb layers with strong perpendicular magnetic anisotropy. *Appl. Physc. Rev.* **9**:021402. DOI:10.1063/5.0087260
48. Krishnia S., Haltz E., Berges L., et al. (2021). Spin-orbit coupling in single-Layer ferrimagnets: direct observation of spin-orbit torques and chiral spin textures. *Phys. Rev. Appl.* **16**:024040. DOI:10.1103/PhysRevApplied.16.024040
49. Nguyen M.-H., Ralph D. C. and Buhrman R. A. (2016). Spin torque study of the spin Hall conductivity and spin diffusion length in Platinum thin films with varying resistivity. *Phys. Rev. Lett.* **116**:126601. DOI:10.1103/PhysRevLett.116.126601
50. Zhu L., Ralph D. C. and Buhrman R. A. (2021). Maximizing spin-orbit torque generated by the spin Hall effect of Pt. *Appl. Physc. Rev.* **8**:031308. DOI:10.1063/5.0059171
51. Xu T., Cheng Y., Dong Y., et al. (2023). Evolution of compensated magnetism and spin-torque switching in ferrimagnetic $Fe_{1-x}Tb_x$. *Phys. Rev. Appl.* **19**:034088. DOI:10.1103/PhysRevApplied.19.034088
52. Lyalin I. and Kawakami R. K. (2024). Interface transparency to orbital current. *Phys. Rev. B* **110**:104418. DOI:10.1103/PhysRevB.110.104418
53. Hayashi M., Kim J., Yamanouchi M., et al. (2014). Quantitative characterization of the spin-orbit torque using harmonic Hall voltage measurements. *Phys. Rev. B* **89**:144425. DOI:10.1103/PhysRevB.89.144425
54. Garello K., Miron I. M., Avci C. O., et al. (2013). Symmetry and magnitude of spin–orbit torques in ferromagnetic heterostructures. *Nat. Nanotechnol.* **8**:587–593. DOI:10.1038/nnano.2013.145
55. Kim J., Sinha J., Hayashi M., et al. (2013). Layer thickness dependence of the current-induced effective field vector in Ta/CoFeB/MgO. *Nat. Mater.* **12**:240–245. DOI:10.1038/nmat3522
56. Avci C. O., Garello K., Gabureac M., et al. (2014). Interplay of spin-orbit torque and thermoelectric effects in ferromagnet/normal-metal bilayers. *Phys. Rev. B* **90**:224427. DOI:10.1103/PhysRevB.90.224427
57. Fan Y., Upadhyaya P., Kou X., et al. (2014). Magnetization switching through giant spin–orbit torque in a magnetically doped topological insulator heterostructure. *Nat. Mater.* **13**:699–704. DOI:10.1038/nmat3973
58. Shao Q., Yu G., Lan Y.-W., et al. (2016). Strong Rashba-Edelstein effect-induced spin–orbit torques in monolayer transition metal dichalcogenide/ferromagnet bilayers. *Nano Lett.* **16**:7514–7520. DOI:10.1021/acs.nanolett.6b03300
59. Wu H., Xu Y., Deng P., et al. (2019). Spin-orbit torque switching of a nearly compensated ferrimagnet by topological surface states. *Adv. Mater.* **31**:1901681. DOI:10.1002/adma.201901681
60. Wu H., Zhang P., Deng P., et al. (2019). Room-temperature spin-orbit torque from topological surface states. *Phys. Rev. Lett.* **123**:207205. DOI:10.1103/PhysRevLett.123.207205
61. Park S. R., Kim C. H., Yu J., et al. (2011). Orbital-angular-momentum based origin of Rashba-type surface band splitting. *Phys. Rev. Lett.* **107**:156803. DOI:10.1103/PhysRevLett.107.156803
62. Park J.-H., Kim C. H., Rhim J.-W., et al. (2012). Orbital Rashba effect and its detection by circular dichroism angle-resolved photoemission spectroscopy. *Phys. Rev. B* **85**:195401. DOI:10.1103/PhysRevB.85.195401
63. Go D., Hanke J.-P., Buhl P. M., et al. (2017). Toward surface orbitronics: giant orbital magnetism from the orbital Rashba effect at the surface of sp-metals. *Sci. Rep.* **7**:46742. DOI:10.1038/srep46742
64. Go D., Jo D., Gao T., et al. (2021). Orbital Rashba effect in a surface-oxidized Cu film. *Phys. Rev. B* **103**:L121113. DOI:10.1103/PhysRevB.103.L121113
65. Finley J. and Liu L. (2016). Spin-orbit-torque efficiency in compensated ferrimagnetic Cobalt-Terbium alloys. *Phys. Rev. Appl.* **6**:054001. DOI:10.1103/PhysRevApplied.6.054001
66. Mishra R., Yu J., Qiu X., et al. (2017). Anomalous current-induced spin torques in ferrimagnets near compensation. *Phys. Rev. Lett.* **118**:167201. DOI:10.1103/PhysRevLett.118.167201
67. Baek S.-h. C., Amin V. P., Oh Y.-W., et al. (2018). Spin currents and spin–orbit torques in ferromagnetic trilayers. *Nat. Mater.* **17**:509–513. DOI:10.1038/s41563-018-0041-5

FUNDING AND ACKNOWLEDGMENTS

This work was supported by the National Natural Science Foundation of China (12404148, 12241406), the National Key R&D Program of China (Grant No. 2022YFA1403603), the National Natural Science Funds for Distinguished Young Scholar (52325105), the CAS Project for Young Scientists in Basic Research (YSBR-084), the Strategic Priority Research Program of the Chinese Academy of Sciences (Grant No. XDB33030100), the Chinese Academy of Sciences under contract No. JZHKYPT-2021-08. Guangdong Basic and Applied Basic Research Foundation, No. 2023A1515012300. The funders had no role in study design, data collection and analysis, decision to publish, or preparation of the manuscript.

AUTHOR CONTRIBUTIONS

T.X. and H.D. initiated the project and supervised the study. T.X., A.T. and K.W. grew the magnetic multilayers and fabricated the Hall bar devices. T.X. and A.T. characterized their electrical and magnetic properties. T.X. performed the current-induced switching and harmonic Hall measurements. T.X. and W.W. conducted the STEM and EDS measurements. T.X., Y.L. and H.D. wrote the manuscript with inputs from all authors. All authors contributed to the manuscript and approved the final version.

DECLARATION OF INTERESTS

The authors declare no competing interests.

DATA AND CODE AVAILABILITY

The authors declare that the main data supporting the present study are available within the main text and Supplemental Information. Extra data are available on reasonable request from the corresponding author.

SUPPLEMENTAL INFORMATION

It can be found online at https://doi.org/10.59717/j.xinn-mater.2025.100158